DØ Note 5468-CONF

Search for squark production in events with jets, hadronically decaying taus and missing transverse energy with the DØ detector at $\sqrt{s}$=1.96 TeV in the Run IIa data

The DØ Collaboration
URL: http://www-d0.fnal.gov

(Dated: August 1, 2007)

A search for squarks is performed in the topology of multijet events accompanied by large missing transverse energy and at least one tau lepton decaying hadronically. Approximately 1 fb^{-1} of $p\bar{p}$ collision data from the Tevatron collider at Fermilab at a center-of-mass energy of 1.96 TeV recorded by the DØ detector is analysed. No evidence of physics beyond the Standard Model is found and lower limits on the squark mass up to 366 GeV are derived in the framework of minimal supergravity with parameters enhancing final states with taus.

Preliminary Results for Summer 2007 Conferences

I. INTRODUCTION

Supersymmetric extensions (SUSY) of the standard model (SM) predict the existence of scalar quarks ($\tilde{q}$), or squarks, and spin-1/2 gluinos ($\tilde{g}$), the supersymmetric partners of quarks and gluons. These colored particles, if sufficiently light, could be copiously produced at hadron colliders. At the Tevatron, previous searches for squarks and gluinos assuming R-parity conservation were performed using events with jets accompanied with large missing transverse energy [1–4], arising mainly from the undetected lightest suspersymmetric particle (LSP) taken as the lightest neutralino ($\tilde{\chi}_1^0$).

However, in some region of parameter space, squarks decay to neutralinos ($\tilde{\chi}_2^0$) or charginos ($\tilde{\chi}_1^\pm$), formed by the supersymmetric partners of the Higgs fields and SM gauge bosons, leading to final states with leptons. The mass difference between SUSY partners of leptons (sleptons) depends on the lepton mass and on parameters of the model, in particular $\tan\beta$ (the ratio of the neutral Higgs vacuum expectation values). Thus, in a given model, the lightest supersymmetric partners of taus ($\tilde{\tau}_1^\pm$) might be the lightest of all sleptons favouring final states with tau leptons *via* the subsequent decay $\tilde{\tau}_1^\pm \to \tau^\pm \tilde{\chi}_1^0$. Other leptonic decay (to electrons and muons) would then be suppressed. Such a mass hierarchy and decay chain are favoured for low slepton mass. In this region, squarks are lighter than gluinos and squark pair production $p\bar{p} \to \tilde{q}_R \tilde{q}_L$ dominates. Fig. 1 illustrates squark pair production and the typical decay chain into tau final states. These events are signed by the presence of two (or more) jets, large missing transverse energy ($\not\!\!E_T$) and at least one tau lepton. Decays *via* a $\tilde{\chi}_1^\pm$ contribute $\sim 2/3$ of the time and lead to the production of one single tau, while decays *via* a $\tilde{\chi}_2^0$ contribute for the rest and lead to the production of two taus. Such signatures have not been exploited yet for a search for supersymmetry at the Tevatron.

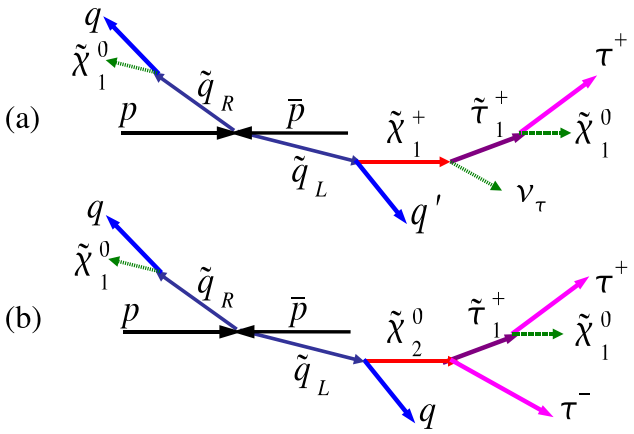

FIG. 1: Scheme of pair produced squarks decaying into leptons, taus are taken as an example. One tau or two taus are produced if squarks decay through a $\tilde{\chi}_1^\pm$ (a) or a $\tilde{\chi}_2^0$ (b) respectively.

The following reports on a search for final states containing jets, at least one tau decaying hadronically and large missing transverse energy using approximately 1 fb^{-1} of data collected at a center-of-mass energy of $\sqrt{s} = 1.96$ TeV with the upgraded DØ detector during the Run IIa phase of the Fermilab Tevatron collider. The second tau produced in the $\tilde{\chi}_2^0$ decay is not identified in order to avoid additional loss in signal efficiency. Squark production is investigated in the framework of minimal supergravity (mSUGRA) [5] in a model with enhanced tau final states.

II. DETECTOR AND DATA SET

A detailed description of the DØ detector can be found in [6]. The central tracking system comprises a silicon microstrip tracker (SMT) and a central fiber tracker (CFT), both located within a 2 T superconducting solenoidal magnet. The SMT and CFT designs were optimised to provide precise tracking and vertexing capabilities over the pseudorapidity range $|\eta| < 2.5$, where $\eta = -\ln[\tan(\theta/2)]$ and θ is the polar angle with respect to the proton beam direction. A liquid-argon and uranium calorimeter covers pseudorapidity up to $|\eta| \approx 4.2$. The calorimeter consists of three sections, housed in separate cryostats: the central one covers $|\eta| \lesssim 1.1$ and the two end sections extend the coverage to larger $|\eta|$. The calorimeter is extended in depth, with four electromagnetic (EM) layers followed by up to five hadronic layers. It is also segmented in projective towers of size 0.1×0.1 in η-ϕ space, where ϕ is the azimuthal angle. Calorimeter cells are defined as intersection of towers and layers. Additional sampling is provided by

scintillating tiles in the region at the boundary between cryostats. An outer muon system, covering $|\eta| < 2$, consists of a layer of tracking detectors and scintillation trigger counters in front of 1.8 T toroids, followed by two similar layers after the toroids. Jets are reconstructed from the energy deposited in calorimeter towers using the Run II cone algorithm [7] with radius $R = \sqrt{(\Delta\phi)^2 + (\Delta\eta)^2} = 0.5$. A minimum transverse energy of 13 GeV per jet is required. The jet energy scale (JES) is derived from the transverse momentum balance in photon-plus-jet events [8]. The $\not\!\!E_T$ is calculated from all cells, and corrected for the jet energy scale and the reconstructed muons. Hadronically decaying taus are characterised by a narrow isolated jet with low track multiplicity [9]. They are found by constructing a calorimeter cluster made of all towers around a seed tower within $R < 0.5$. Only clusters with a transverse energy (E_T) greater than 5 GeV and associated with a track of transverse momentum (p_T) above 1.5 GeV with $R < 0.3$ are kept. Additional tracks are added if the invariant mass of tracks is compatible with the tau mass. EM subclusters of minimum transverse energy of 800 MeV are constructed from cells of the calorimeter EM sections belonging to the tau cluster. Taus are classified in three types: 1) a single track with no EM subclusters, the typical signature of $\tau^\pm \to \pi^\pm \nu_\tau$; 2) a single track with at least one EM subcluster, the typical signature of $\tau^\pm \to \pi^\pm \pi^0 \nu_\tau$; 3) two or three tracks associated with or without EM subclusters, the typical signature of $\tau^\pm \to \pi^\pm \pi^\mp \pi^\pm (\pi^0) \nu_\tau$. The tau energy is inferred from the transverse momenta of the associated central tracks, the E_T calorimeter cluster and the known calorimeter response to $\pi^\pm$ parametrised as a function of track p_T and η.

For the search reported in this document, data collected by the DØ experiment during the Run IIa of the Tevatron, from April 2003 through February 2006, are analysed. This data sample corresponds to an integrated luminosity of 0.96±0.06 fb^{-1} [10] after requiring data of good quality. Events were recorded using acoplanar dijet and multijet triggers requiring missing transverse energy calculated using the sum of the jet momenta ($\not\!\!H_T = |\Sigma_{jets} \overrightarrow{p_T}|$). The DØ trigger system consists of three level, L1, L2 and L3. Events were required to have at least three calorimeter towers of size $\Delta\phi \times \Delta\eta = 0.2 \times 0.2$ with transverse energy greater than 5 GeV. For the acoplanar dijet trigger, $\not\!\!H_T$ was required to be greater than 20 GeV (30 GeV) and the acoplanarity (defined as the azimuthal angle between the two leading jets, ordered in decreasing E_T), to be less than 168.75° (170°) at L2 (L3). For the multijet trigger, at least three jets were required at L2 and, at L3, events were required to have $H_T = \sum_{\text{jets}} E_T$ and $\not\!\!H_T$ greater than 125 GeV and 25 GeV respectively. In the last third of the data sample (recorded at higher instantaneous luminosities), additional L3 requirements were performed in those triggers to reduce their online rate: in the acoplanar dijet trigger the minimal azimuthal angle between the $\not\!\!H_T$ direction and any jet was required to be greater than 25°, rejecting events with mismeasured jet energy; and three jets with E_T above 20 GeV were required in the multijet trigger.

III. MODELLING OF SIGNAL AND STANDARD MODEL BACKGROUND EVENTS

The signal topology consists of jets, $\not\!\!E_T$ and at least one tau. This topology also arises from SM processes involving W and Z bosons (including top quark production and decay) where one tau is produced. Events with fake taus (coming from misidentified electrons, muons or jets) and fake $\not\!\!E_T$ (created by jet energy mismeasurement for example) from sources such as multijet (QCD process events) also contribute. Signal efficiencies and yields for standard model background events are evaluated using Monte Carlo techniques, except multijet backgrounds which are not simulated. Generated events are subjected to a detailed GEANT-based [11] simulation of the detector geometry and response and processed through the same reconstruction chain as data.

W (+jets) $\to \ell\nu$, $\gamma^\star/Z$ (+jets) $\to \ell\ell$ and $t\bar{t}$ (+jets) are generated with ALPGEN version 2.05 [12] interfaced with PYTHIA 6.3 [13] for the simulation of initial and final state radiation, and of parton hadronisation. Heavy flavor and light flavor quark contributions are generated separately. Tau decays are simulated with the generator TAUOLA [14] and the CTEQ6L1 [15],[16] parton density functions (PDF) are used. Absolute cross-section normalisation is performed using NLO K-factors computed with MCFM [17]. Inclusive diboson production is generated with PYTHIA and single top with COMPHEP [18].

Squark (including all species except stops) and gluino production and inclusive cascade decay are simulated with PYTHIA 6.3. Sparticle mass and couplings are computed with SUSPECT 2.3 [19] and SDECAY 1.1a [20] from a set of five mSUGRA parameters: m_0 and $m_{1/2}$, the universal scalar and gaugino masses, and A_0, a universal trilinear coupling, all defined at the grand unification scale; $\tan\beta$ and the sign of the Higgs-mixing mass parameter μ. In order to enhance the stau mass matrix mixing and extend the region of final states with taus, a high value of $\tan\beta = 15$ is fixed. A_0 is set to $-2\ m_0$ to favour high Higgs boson masses and the sign of μ is negative. Fig. 2 illustrates the region of the (m_0, $m_{1/2}$) space with enhanced branching fraction to taus in this model. Squark and gluino masses are shown on the same figure. Signal samples are normalised to the NLO cross-section computed with PROSPINO 2 [21] and the CTEQ6.1M PDF set. The signal cross section is typically of 0.3 pb for squark masses of about 350 GeV.

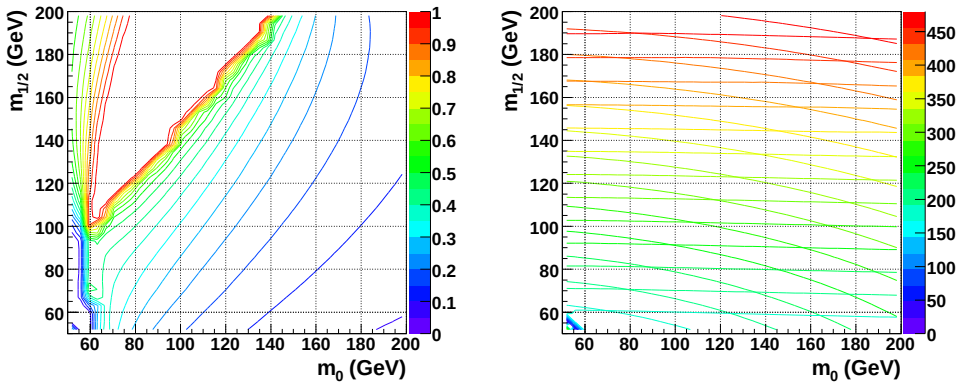

FIG. 2: In the (m_0, $m_{1/2}$) plane of the mSUGRA model with $\tan\beta = 15$, $A_0 = -2m_0$ and $\mu < 0$, (left): BR($\tilde{\chi}_1^{\pm} \to \tau^{\pm}\tilde{\chi}_1^0\nu_\tau$); (right) almost horizontal curves are the gluino iso-masses and other curves are the squark iso-masses, averaged over 10 squark species (stops are excluded).

IV. EVENT SELECTION

First a common preselection and a selection based on jets and $\not\!\!E_T$ objects, shared with the generic search for squarks and gluinos [4] in the Jets and $\not\!\!E_T$ signature, are applied. The identification of one tau candidate is performed afterwards.

The preselection criteria are summarised in Table I. Preselected events are required to have a substantial $\not\!\!E_T$ (≥ 40 GeV) and to have at least two reconstructed jets. Events must be acoplanar. The longitudinal position of the primary vertex (PV) is restricted to be central in the detector in order to reduce bad primary vertex reconstruction. The two leading jets are required to be in the central region of the calorimeter ($|\eta_{det}| < 0.8$, where η_{det} is calculated under the assumption the jet originates from the center of the detector) and to be energetic ($E_T \geq 35$ GeV). The tracking capabilities of the DØ detector at the Run II are used to significantly reduce QCD backgrounds with jet transverse energy mismeasurement due to a wrong vertex choice. The fraction of charged particle transverse momenta associated to the jet (in a cone with $R = 0.5$) and pointing to the PV, compared the transverse momenta of those pointing to any vertex ($CPF0$) is used to this end.

Two analyses are performed in order to take profit of the different signal topologies firing the acoplanar dijet trigger or the multijet trigger. Criteria used in each analysis stream (JT1 and JT2 respectively) are summarised in Table I. In both analyses, the $\not\!\!E_T$ requirement is tightened to 75 GeV to reject most of the multijet background (mainly from QCD processes), as indicated on Fig. 3. The direction of the $\not\!\!E_T$ is required to be away in azimuth from the two leading jets. This removes events where mismeasured jet energy creates $\not\!\!E_T$ aligned with the jet. In the JT1 analysis, this instrumental background is further reduced by requiring a minimal value of the azimuthal angle between any reconstructed jet and the $\not\!\!E_T$ of 40°. Due to the high jet multiplicity in the JT2 analysis stream this criteria is not applied but a third jet with $E_T \geq 35$ GeV in the acceptance of the tracker ($|\eta_{det}| < 2.5$) is required, and H_T must be greater than 200 GeV.

Events are required to contain at least one tau candidate separated from the two leading jets ($\Delta R(\tau, \mathrm{jet}_{1,2}) \geq 0.5$). The tau candidate must lie in the pseudorapidity range $|\eta_{\mathrm{det}}| \leq 2.5$. Its transverse momentum must exceed 15 GeV and the transverse momentum of the associated track is required to be $p_T \geq 4$ GeV for tau-type 1. In the case of tau-type 3, the scalar sum of transverse momenta of all tracks associated to the tau must be greater than 8 GeV. Jets originating from quarks and gluons fake hadronically decaying taus and a set of neural networks (NN_{jet}), one for each tau-type, has been developed to discriminate between them. They exploit the differences in transverse and longitudinal shower shape, as well as differences in the isolation in the calorimeter and in the tracker. Training is performed using simulated taus as signal and multijet events from data as background. Output variables peak near one for real taus and zero for fake taus. This analysis uses moderate NN_{jet} cut values (0.4/0.5/0.6 for tau-type 1/2/3) to insure a high background rejection while keeping a high selection efficiency for hadronically decaying taus. Other discriminating variables like $\not\!\!E_T$ and H_T are used later to optimise the selection and reject remaining backgrounds coming from multijet processes. Electrons are generally identified as a tau-type 2 and a neural network (NN_{elec}) similar to the NN_{jet} has been developed to discriminate between them (training is performed using simulated $Z \to ee$

TABLE I: Selection criteria of both JT1 and JT2 analyses.

Preselection	All analyses	
$\not\!\!E_T$	$\geq$ 40 GeV	
number of reconstructed jets	≥ 2	
acoplanarity	$< 165^\circ$	
$\lvert \mathrm{PV}_z \rvert$	< 60 cm	
1$^{\mathrm{st}}$ leading jet E_T, $\lvert\eta_{det}\rvert$, $CPF0$	$\geq$ 35 GeV , ≤ 0.8 , $\geq 85\%$	
2$^{\mathrm{nd}}$ leading jet E_T, $\lvert\eta_{det}\rvert$, $CPF0$	$\geq$ 35 GeV , ≤ 0.8 , $\geq 85\%$	
Jets and $\not\!\!E_T$ selection	JT1 analysis	JT2 analysis
trigger	acoplanar dijet	multijet
$\not\!\!E_T$	$\geq$ 75 GeV	$\geq$ 75 GeV
$\Delta\Phi(\not\!\!E_T, \mathrm{jet}_1)$	$\geq 90^\circ$	$\geq 90^\circ$
$\Delta\Phi(\not\!\!E_T, \mathrm{jet}_2)$	$\geq 50^\circ$	$\geq 50^\circ$
$\Delta\Phi_{min}(\not\!\!E_T, \text{any jet})$	$\geq 40^\circ$	-
number of reconstructed jets	-	≥ 3
3$^{\mathrm{rd}}$ leading jet E_T, $\lvert\eta_{det}\rvert$	-	$\geq$ 35 GeV , ≤ 2.5
H_T	-	$\geq$ 200 GeV
Tau candidate selection	All analyses	
number of tau candidate	≥ 1	
$\Delta R(\tau_{\mathrm{cand}}, \mathrm{jet}_1)$	≥ 0.5	
$\Delta R(\tau_{\mathrm{cand}}, \mathrm{jet}_2)$	≥ 0.5	

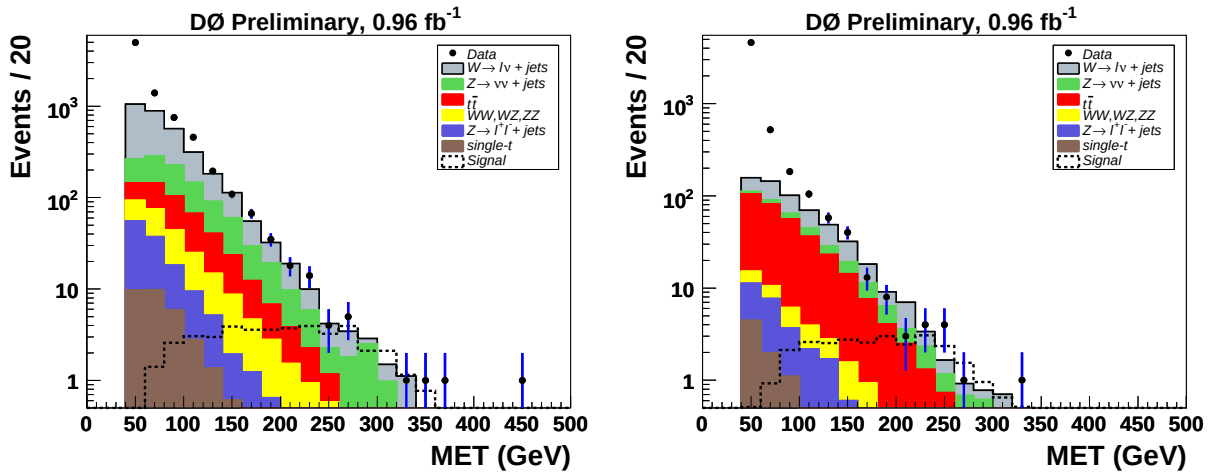

FIG. 3: $\not\!\!E_T$ distributions for events after the Jets+$\not\!\!E_T$ selection in the analyses JT1 (left) and JT2 (right). $\not\!\!E_T$ cuts are relaxed to 40 GeV. The signal point (m_0,$m_{1/2}$)=(100,150) GeV is superimposed.

as background). A moderate cut at 0.3 is applied. Electrons tend to fake tau-type 1 candidates in the region of the DØ detector not instrumented for measuring EM energy deposition. Therefore, this region ($1.1 < |\eta^{\tau}_{det}| < 1.5$)) is cut away for tau-type 1 candidates. Muons can be misidentified as one-prong hadronic tau decay as well. In particular, muon contribution is reduced by comparing the energy measured in the calorimeter and the tau associated track momentum ($E/p \geq 0.7$). This cut is not applied for tau-type 2. The DØ calorimeter is dense and muons interacting by Bremsstrahlung are removed by requiring the fraction of energy deposited in the last section of the calorimeter to be less than 40%.

As indicated on Fig. 4, the excess of data at low $\not\!\!E_T$ comes from multijet background events which are not simulated. The overall SM predictions are in good agreement with data for $\not\!\!E_T$ above ~125 GeV, and even lower for the JT1 analysis. As shown in Fig. 5, the shapes of key variables are also in good agreement with predictions. This figure

includes the distribution of the variable $JJTH_T = E_T^{\rm jet_1} + E_T^{\rm jet_2} + E_T^{\tau_{\rm cand}}$, characteristic of the signal and used later to separate optimally signal and backgrounds. Variables that depend on angular correlations are also well described. As an example, the transverse mass of the $(\tau_{\rm cand}, \not\!\!E_T)$ system has been included in the figure. It exhibits the typical Jacobian edge of the W transverse mass shape as expected at this background dominated stage of the analysis.

V. SELECTION OPTIMISATION

Two final cuts on $JJTH_T$ and $\not\!\!E_T$ are optimised by minimising the expected upper limit on the cross section in the absence of signal. To this end, as well, as for the derivation of the final results, the modified frequentist CL_s method is used [22], [23]. Multijet backgrounds are not simulated. However, for high cuts on $JJTH_T$ and $\not\!\!E_T$ the expected contribution is negligible and it is conservatively neglected in the following. Giving emphasis to the high squark mass region, the optimisation is performed on each analysis stream separately and on a combination of both (events selected by either of the analyses enter in the combination). The optimal sensitivity is obtained for the analysis combination with additional cuts of $JJTH_T \geq 325$ GeV and $\not\!\!E_T \geq 175$ GeV.

Statistical and systematics uncertainties are included in the CL_s computation. The uncertainty due to the JES corrections is the most important. It is 15% for the background and 10% for the signal. The uncertainties on jet reconstruction and identification efficiency, on the jet energy resolution and on the $CPF0$ lead to systematic uncertainties of 1%, 2% and 5% respectively. The uncertainties on the tau reconstruction and efficiency, on the tau energy scale corrections and on the neural net outputs are 3%, 4% (this value is 2% for signal events) and 2% respectively. The uncertainty on the determination of the luminosity is 6.1% [10] and the trigger uncertainty is 2%. The uncertainty on the signal acceptance due to the choice of the PDF set was determined to be 6% [3]. All these uncertainties are fully correlated between signal and SM backgrounds. A 15% uncertainty is set on the SM background cross-sections.

The number of events selected by each analysis and by the combination are given in Table II. Combining analyses, two data events are selected, in good agreement with the SM expectations. The main background contributions arise from top pair and W(+jets) production processes. Table II reports on the number of expected events for two signal points. The one at $(m_0, m_{1/2}) = (80, 160)$ GeV, is close to the indirect LEP exclusion limits [24] and corresponds to high squark masses (around 375 GeV). The other one, at $(m_0, m_{1/2}) = (100, 150)$ GeV, has a peculiar mass hierarchy where the $\tilde{\tau}_1^{\pm}$ is a few GeV lighter than the $\tilde{\chi}_2^0$. In this configuration the lepton coming from the $\tilde{\chi}_2^0$ decay is very soft and mostly undetectable. Such mass configurations are very difficult to detect in a direct search for $\tilde{\chi}_1^{\pm}\tilde{\chi}_2^0$ production in the three lepton final states. This analysis is sensitive to both points with expected CLs values less than 5%. Final distributions of $JJTH_T$ and $\not\!\!E_T$ are displayed on Fig. 6 where signal point (100, 150) expectations are shown above the SM predictions. Event displays of the candidate with the highest $\not\!\!E_T$ are shown in Fig. 7 and its kinematics properties are reported in Table III.

TABLE II: Number of events observed in data, expected in SM and for two signal points, given in $(m_0, m_{1/2})$ values, for each analysis stream with $JJTH_T \geq 325$ GeV and $\not\!\!E_T \geq 175$ GeV cuts. Errors quoted on signals are statistical only. Expected CLs values are given in brackets.

Analysis	Data	SM predictions	Signal (80, 160)	Signal (100, 150)
OR	2	1.68 ± 0.24 (stat.) $^{+0.55}_{-0.31}$ (syst.)	[0.0333] 4.73 ± 0.37	[0.0064] 7.08 ± 0.57
JT1	1	0.57 ± 0.14 (stat.) $^{+0.20}_{-0.12}$ (syst.)	[0.0783] 2.65 ± 0.28	[0.0277] 3.86 ± 0.43
JT2	1	1.38 ± 0.22 (stat.) $^{+0.40}_{-0.23}$ (syst.)	[0.1074] 3.27 ± 0.31	[0.0235] 5.39 ± 0.50

VI. INTERPRETATION IN MSUGRA

Limits are derived at 95% C.L. At present theoretical uncertainties on the squark-pair production cross-sections due to the choice of the PDF set and on the renormalisation and factorisation scale are not taken into account.

In the region where $\tilde{\chi}_1^{\pm}$ and $\tilde{\chi}_2^0$ decay exclusively into tau final states (at low m_0), the analysis sensitivity is kinematically limited by the squark mass (at high $m_{1/2}$). For large slepton masses, $\tilde{\chi}_1^{\pm}$ and $\tilde{\chi}_2^0$ decay through a virtual W or Z leading to final states to taus according to the SM boson branching fractions. This analysis is sensitive to part of this region (if squarks are sufficiently light to be abundantly produced), but it is already excluded by the indirect search for chargino from LEP. Therefore, results of this analysis, in term of exclusion, is restricted to the region of interest of enhanced final states to taus.

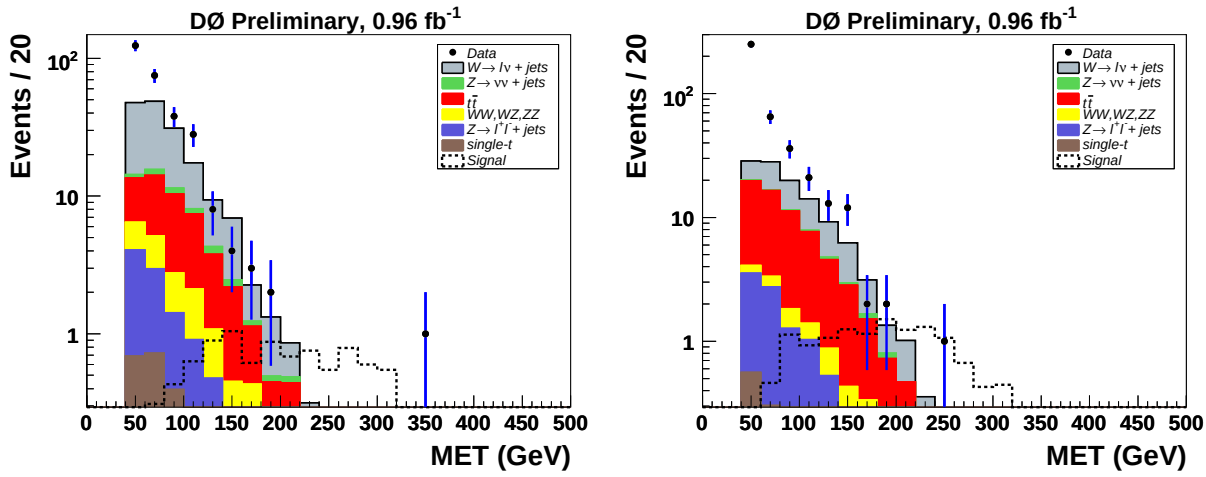

FIG. 4: $\not\!\!E_T$ of events passing the tau selection in the analyses JT1 (left) and JT2 (right). $\not\!\!E_T$ cuts are relaxed to 40 GeV. The signal point (m_0,$m_{1/2}$)=(100,150) GeV is superimposed.

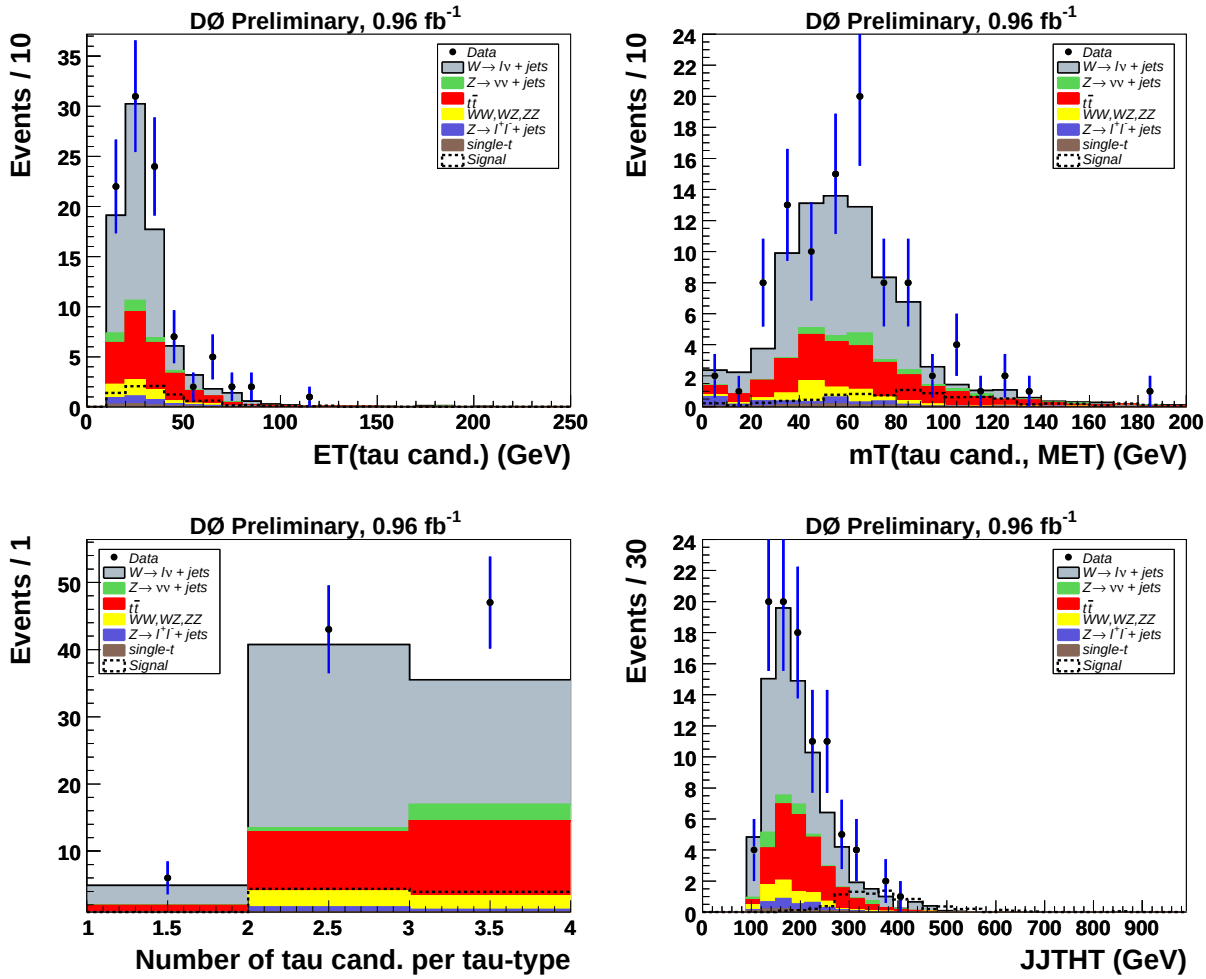

FIG. 5: After the tau selection in the JT1 analysis, from left to right and top to bottom: transverse energy of tau candidates, ($\tau_{cand}\not\!\!E_T$) transverse mass, number of tau candidates per tau-type and $JJTH_T$. The signal point (m_0,$m_{1/2}$)=(100,150) GeV is superimposed.

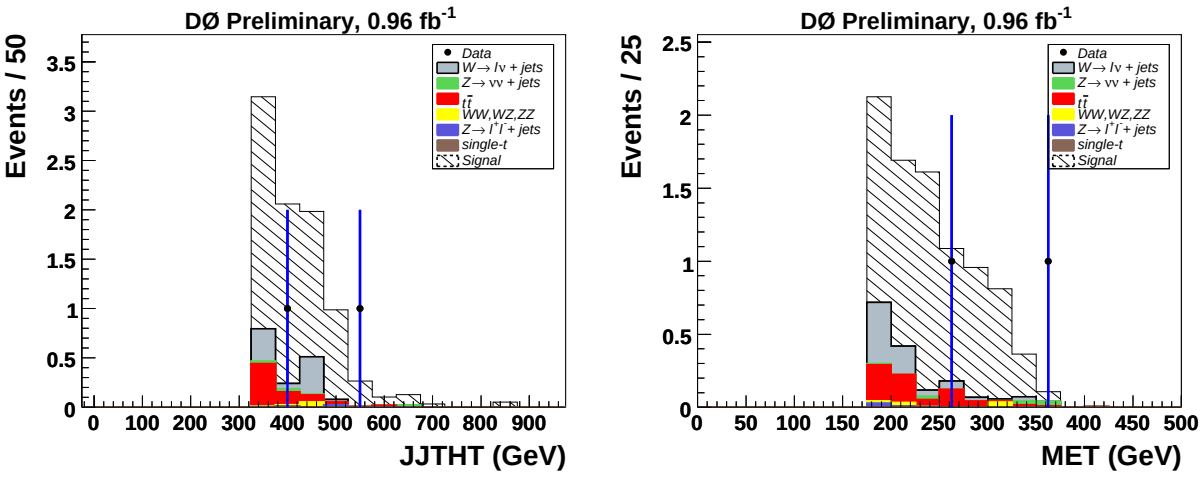

FIG. 6: Final distributions of $JJTH_T$ (left) and $\not\!\!E_T$ (right) for the signal point (m_0, $m_{1/2}$) = (100, 150) GeV with the two analysis streams combined with an "OR" and additional cuts $JJTH_T \geq 325$ GeV and $\not\!\!E_T \geq 175$ GeV. Signal events are displayed on top of the background expectations.

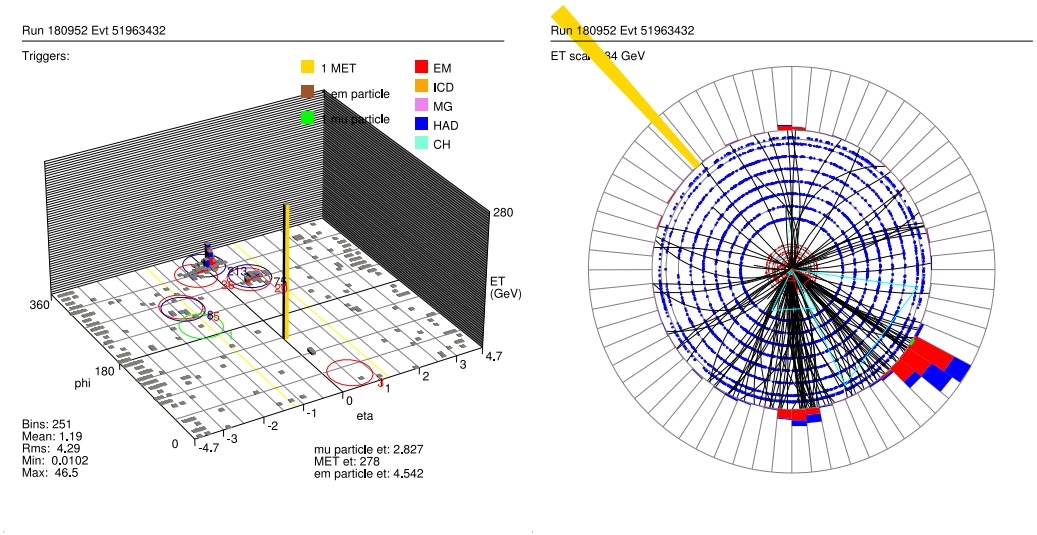

FIG. 7: Lego plot of the calorimeter energy deposition in the η-ϕ plane (left) and x-y view (z being along the beam axis) of the candidate event with highest $\not\!\!E_T$.

TABLE III: Kinematic properties of the candidate event with the highest $\not\!\!E_T$. Energies are given in GeV and angles in radians.

Object	E_T	η	ϕ
Jet 1	266.	−0.21	5.7
Jet 2	106.	0.54	4.8
Jet 3	15.	−1.54	4.3
Tau 1 (type: 3)	15.	−0.09	1.6
H_T	386.		
$JJTH_T$	387.		
$\not\!\!E_T$	353.		
EM particle	14.	−0.05	1.5

Figure 8 shows the resulting expected and observed lower limits in the (m_0, $m_{1/2}$) plane of the mSUGRA framework with $\tan\beta = 15$, $A_0 = -2m_0$ and $\mu < 0$. This analysis excludes squark masses (averaged over 10 squarks species) up to 366 GeV (the expected limit is 373 GeV) at the highest m_0 value of the limit contour. For reference, the generic search for squarks and gluinos performed by DØ on the same dataset in the Jets+$\not\!\!E_T$ signature [4] in the mSUGRA framework with $\tan\beta = 3$, $A_0 = 0$ and $\mu < 0$, and where final states to taus are not explored, set an absolute expected lower limit on squark masses of 384 GeV. The results of this analysis also constrain the mSUGRA parameters at the grand unification scale. For m_0 value between 80 and 110 GeV, the expected limit on $m_{1/2}$ reaches values about 15 GeV above the indirect limit from the LEP2 chargino search.

VII. CONCLUSION

Squark pair production is searched for in events with jets, tau(s) decaying hadronically and large missing transverse energy using all DØ data recorded at a center-of-mass energy of 1.96 TeV during the Run IIa phase of the Tevatron. No evidence for signal is observed in this 1 fb^{-1} data sample. The result of this search is interpreted in term of exclusion on the mSUGRA model parameter space for $\tan\beta = 15$, $A_0 = -2m_0$ and $\mu < 0$ enhancing final states to taus. The highest excluded squark mass at 95% C.L is 366 GeV. This search is the first one to explore supersymmetric models in tau final states accompanied with jets at the Tevatron. It is important to complement other searches, such as the generic search for squarks and gluinos in events with jets and large $\not\!\!E_T$ or direct search for chargino-neutralino production in the tri-lepton final state where one lepton could be kinematically undetectable.

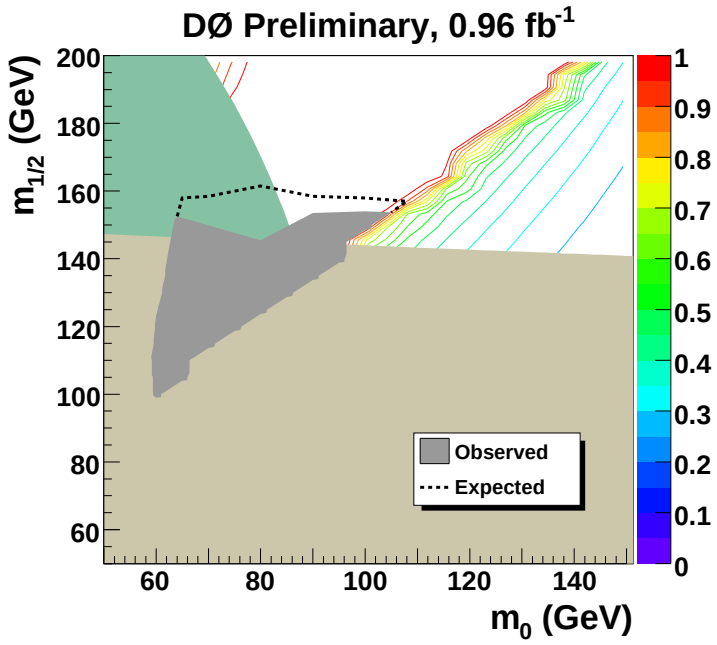

FIG. 8: Expected and observed limits set by this analysis at 95% C.L. in the (m_0, $m_{1/2}$) plane of the mSUGRA model with $\tan\beta = 15$, $A_0 = -2\,m_0$ and $\mu < 0$. The green and beige plain areas are respectively excluded by LEP2 slepton ($m_{\tilde{e}} > 100$ GeV, $m_{\tilde{\mu}} > 97$ GeV and $m_{\tilde{\tau}} > 93$ GeV) and chargino ($m_{\tilde{\chi}^\pm} > 103$ GeV) searches. The thin colored lines represent the isocurves of the branching fraction of $\tilde{\chi}_1^\pm$ decaying in to $\tau^\pm\tilde{\chi}_1^0\nu_\tau$.

Acknowledgments

We thank the staffs at Fermilab and collaborating institutions, and acknowledge support from the DOE and NSF (USA); CEA and CNRS/IN2P3 (France); FASI, Rosatom and RFBR (Russia); CAPES, CNPq, FAPERJ, FAPESP and FUNDUNESP (Brazil); DAE and DST (India); Colciencias (Colombia); CONACyT (Mexico); KRF and KOSEF (Korea); CONICET and UBACyT (Argentina); FOM (The Netherlands); Science and Technology Facilities Council (United Kingdom); MSMT and GACR (Czech Republic); CRC Program, CFI, NSERC and WestGrid Project (Canada); BMBF and DFG (Germany); SFI (Ireland); The Swedish Research Council (Sweden); CAS and CNSF (China); Alexander von Humboldt Foundation; and the Marie Curie Program.

[1] S. Abachi *et al.* (DØ Collaboration), Phys. Rev. Lett. **75**, 618 (1995).
[2] B. Abbott *et al.* (DØ Collaboration), Phys. Rev. Lett. **83**, 4937 (1999).
[3] V.M. Abazov *et al.* (DØ Collaboration), Phys. Lett. B **638**, 119 (2006).
[4] DØ Collaboration, DØ Conference Note 5312.
[5] H.P. Nilles, Phys. Rep. **110** (1984) 1.
[6] V.M. Abazov *et al.* (DØ Collaboration), Nucl. Instr. and Methods A **565**, 463 (2006).
[7] G.C. Blazey *et al.*, in Proceedings of the Workshop "QCD and weak bosons physics at the Run II", edited by U. Baur, R.K. Ellis and D. Zeppenfeld (Fermilab, Batavia, Fermilab, 2000), p. 47; see Section 3.5 for details.
[8] V.M. Abazov *et al.* (DØ Collaboration), Phys. Rev. D **75**, 092001 (2007).
[9] C. Galea (DØ Collaboration), FERMILAB-CONF-06-462-E; *a.k.a.* DØ note 5304.
[10] T. Andeen *et al.* (DØ Collaboration), FERMILAB-TM-2365-E (2007); *a.k.a.* DØ note 5398.
[11] R. Brun and F. Carminati, CERN Programm Library Long Writeup W5013, 1993 (unpublished).
[12] M.L. Mangano *et al.*, JHEP **0307** (2003) 001.
[13] T. Sjöstrand *et al.*, Computer Phys. Commun. **135** (2001) 238.
[14] S. Jadach, J.H. Kuhn and Z. Was, Comput. Phys. Commun. **64** (1990) 275.
[15] J. Pumplin *et al.*, JHEP **207** (2002) 012; hep-ph/0201195v3.
[16] D. Stump *et al.*, JHEP **0310** (2003) 046.
[17] J. Campbell and K. Ellis, `http://mcfm.fnal.gov/`
[18] A. Pukhov *et al.*, Preprint INP MSU 98-41/542; hep-ph/9908288.
[19] A. Djouadi, J.-L. Kneur and G. Moultaka, Comput. Phys. Commun. **176** (2007) 426-455; hep-ph/0211331.
[20] M. Muhlleitner, A. Djouadi and Y. Mambrini, Comput. Phys. Commun. **168** (2005) 46-70; hep-ph/0311167.
[21] W. Beenakker, R. Hoepker and M. Spira, Nucl. Phys. B **492** (1997) 51.
[22] T. Junk, Nucl. Instrum. Methods in Phys. Res. A **434**, 435 (1999).
[23] A. Read, in "First Workshop on Confidence Limits", CERN Report No CERN-2000-005, 2000.
[24] LEP SUSY Working group for the ALEPH, DELPHI, L3 and OPAL collaborations, `http://lepsusy.web.cern.ch/lepsusy/`